Paper Number: **360**

Title: **Development of an Input Suite for an Orthotropic Composite Material Model**

Authors : Canio Hoffarth
Loukham Shyamsunder
Bilal Khaled
Subramaniam Rajan
Robert Goldberg
Kelly S. Carney
Paul DuBois
Gunther Blankenhorn

ABSTRACT

An orthotropic three-dimensional material model suitable for use in modeling impact tests has been developed that has three major components – elastic and inelastic deformations, damage and failure. The material model has been implemented as MAT213 into a special version of LS-DYNA and uses tabulated data obtained from experiments. The prominent features of the constitutive model are illustrated using a widely-used aerospace composite – the T800S/3900-2B[P2352W-19] BMS8-276 Rev-H-Unitape fiber/resin unidirectional composite. The input for the deformation model consists of experimental data from 12 distinct experiments at a known temperature and strain rate: tension and compression along all three principal directions, shear in all three principal planes, and off axis tension or compression tests in all three principal planes, along with other material constants. There are additional input associated with the damage and failure models. The steps in using this model are illustrated – composite characterization tests, verification tests and a validation test. The results show that the developed and implemented model is stable and yields acceptably accurate results.

Canio Hoffarth, Arizona State University, Tempe, Arizona 85287, U.S.A.
Loukham Shyamsunder, Arizona State University, Tempe, Arizona 85287, U.S.A.
Bilal Khaled, Arizona State University, Tempe, Arizona 85287, U.S.A.
Subramaniam Rajan, Arizona State University, Tempe, Arizona 85287, U.S.A.
Robert Goldberg, NASA-Glenn Research Center, Cleveland, Ohio, U.S.A.
Kelly S. Carney, George Mason University, Fairfax, Virginia, U.S.A.
Paul DuBois, George Mason University, Fairfax, Virginia, U.S.A.
Gunther Blankenhorn, LSTC, Livermore, California, U.S.A.

INTRODUCTION

In this paper an orthotropic three-dimensional material model that has three major components – elastic and inelastic deformations, damage, and failure, has been developed for use in modeling impact tests [1, 2, 3]. The continuum mechanics based macro model is designed to model structural systems, such as those found in aerospace applications, in a practical and efficient manner. However, using a new constitutive model available in any commercial program is daunting and challenging. We discuss the steps needed to efficiently and accurately use the newly developed material model that has been implemented as MAT213 into a special version of LS-DYNA [4]. It is driven by tabulated data obtained from either actual or virtual experiments [5]. Fig. 1 shows the recommended steps. The initial step is to conduct material characterization tests. As a bare minimum, quasi-static, room temperature (QS-RT) tests are needed to generate the complete stress-strain curves. This data can be supplemented with additional data involving rate and temperature dependencies, coupled and uncoupled damage versus total strain curves and tests to obtain the failure-related parameters.

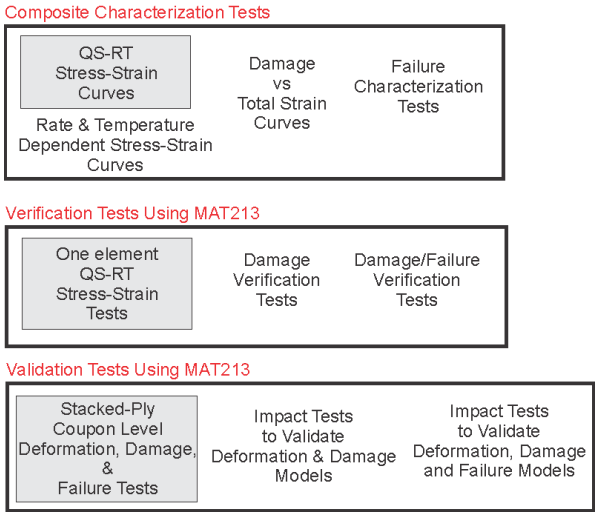

Figure 1. Steps for effectively using MAT213

The next step is to ensure the data is valid by running one or multi-element verification tests with at least the deformation model. Finally, the last step is to ensure that the experimental data and the constitutive model are acceptable by running validation tests. In the rest of the paper, we discuss the highlights of the theory and provide details of the three steps.

ORTHOTROPIC PLASTICITY CONSTITUTIVE MODEL

The developed constitutive model has three components that deal with deformation, damage, and failure. Separating the total composite behavior into these three components allows for the deformation model to capture the elastic and inelastic deformations, the damage model to capture the reduction in stiffness observed during material unloading, and the failure model to determine if finite elements need to be eroded.

Deformation Model: A quadratic yield function which has the form of the commonly used Tsai-Wu composite failure model is used as

$$f(\sigma) = a + \begin{pmatrix} F_1 & F_2 & F_3 & 0 & 0 & 0 \end{pmatrix} \begin{bmatrix} \sigma_{11} \\ \sigma_{22} \\ \sigma_{33} \\ \sigma_{12} \\ \sigma_{23} \\ \sigma_{31} \end{bmatrix} + \begin{bmatrix} \sigma_{11} \\ \sigma_{22} \\ \sigma_{33} \\ \sigma_{12} \\ \sigma_{23} \\ \sigma_{31} \end{bmatrix}^T \begin{bmatrix} F_{11} & F_{12} & F_{13} & 0 & 0 & 0 \\ F_{12} & F_{22} & F_{23} & 0 & 0 & 0 \\ F_{13} & F_{23} & F_{33} & 0 & 0 & 0 \\ 0 & 0 & 0 & F_{44} & 0 & 0 \\ 0 & 0 & 0 & 0 & F_{55} & 0 \\ 0 & 0 & 0 & 0 & 0 & F_{66} \end{bmatrix} \begin{bmatrix} \sigma_{11} \\ \sigma_{22} \\ \sigma_{33} \\ \sigma_{12} \\ \sigma_{23} \\ \sigma_{31} \end{bmatrix} \tag{1}$$

where $a = -1$. The yield function coefficients, F_{ij}, depend on the current yield stress values, determined through the use of tabulated stress-strain curves, and are calculated as

$$\begin{aligned} F_1 &= \frac{1}{\sigma_{11}^T} - \frac{1}{\sigma_{11}^C} & F_{11} &= \frac{1}{\sigma_{11}^T \sigma_{11}^C} & F_{44} &= \frac{1}{\sigma_{12}^2} \\ F_2 &= \frac{1}{\sigma_{22}^T} - \frac{1}{\sigma_{22}^C} & F_{22} &= \frac{1}{\sigma_{22}^T \sigma_{22}^C} & F_{55} &= \frac{1}{\sigma_{23}^2} \\ F_3 &= \frac{1}{\sigma_{33}^T} - \frac{1}{\sigma_{33}^C} & F_{33} &= \frac{1}{\sigma_{33}^T \sigma_{33}^C} & F_{66} &= \frac{1}{\sigma_{31}^2} \end{aligned} \tag{2}$$

$$F_{12} = \frac{2}{\left(\sigma_{12}^{45}\right)^2} - \frac{F_1 + F_2}{\sigma_{12}^{45}} - \frac{1}{2}\left(F_{11} + F_{22} + F_{44}\right) \tag{3}$$

$$F_{23} = \frac{2}{\left(\sigma_{23}^{45}\right)^2} - \frac{F_2 + F_3}{\sigma_{23}^{45}} - \frac{1}{2}\left(F_{22} + F_{33} + F_{55}\right) \tag{4}$$

$$F_{13} = \frac{2}{\left(\sigma_{31}^{45}\right)^2} - \frac{F_1 + F_3}{\sigma_{31}^{45}} - \frac{1}{2}\left(F_{11} + F_{33} + F_{66}\right) \tag{5}$$

where the superscripts T, C and 45 denote data obtained from tension, compression and 45-degree off-axis tests, respectively. A non-associative flow rule is used to compute the evolution of the components of plastic strain and the plastic potential function is defined as

$$h = \sqrt{\begin{aligned} &H_{11}\sigma_{11}^2 + H_{22}\sigma_{22}^2 + H_{33}\sigma_{33}^2 + 2H_{12}\sigma_{11}\sigma_{22} + 2H_{23}\sigma_{22}\sigma_{33} + \\ &2H_{31}\sigma_{33}\sigma_{11} + H_{44}\sigma_{12}^2 + H_{55}\sigma_{23}^2 + H_{66}\sigma_{31}^2 \end{aligned}} \tag{6}$$

where the H_{ij} are the flow rule coefficients that are computed using experimental data.

Damage Model: A semi-coupled, directionally dependent model is used to capture the relationship between true stress and effective stress as

$$\begin{pmatrix}\sigma_{11}\\ \sigma_{22}\\ \sigma_{33}\\ \sigma_{12}\\ \sigma_{23}\\ \sigma_{13}\end{pmatrix}=\begin{bmatrix}M_{11} & 0 & 0 & 0 & 0 & 0\\ 0 & M_{22} & 0 & 0 & 0 & 0\\ 0 & 0 & M_{33} & 0 & 0 & 0\\ 0 & 0 & 0 & M_{44} & 0 & 0\\ 0 & 0 & 0 & 0 & M_{55} & 0\\ 0 & 0 & 0 & 0 & 0 & M_{66}\end{bmatrix}\begin{pmatrix}\sigma_{11}^{eff}\\ \sigma_{22}^{eff}\\ \sigma_{33}^{eff}\\ \sigma_{12}^{eff}\\ \sigma_{23}^{eff}\\ \sigma_{13}^{eff}\end{pmatrix} \tag{7}$$

For example, $M_{11}=M_{11}\left(\varepsilon_{11}^{p},\varepsilon_{22}^{p},\varepsilon_{12}^{p}\right)$ and

$$M_{11}=\left(1-d_{11}^{11}\left(\varepsilon_{11}^{p}\right)\right)\left(1-d_{22}^{11}\left(\varepsilon_{22}^{p}\right)\right)\left(1-d_{33}^{11}\left(\varepsilon_{33}^{p}\right)\right)\left(1-d_{12}^{11}\left(\varepsilon_{12}^{p}\right)\right)\left(1-d_{23}^{11}\left(\varepsilon_{23}^{p}\right)\right)\left(1-d_{13}^{11}\left(\varepsilon_{13}^{p}\right)\right) \tag{8}$$

where the damage parameter d_{ij}^{kl} represents damage in the *kl* due to loading along the *ij* direction, i.e. d_{33}^{11} represents the damage in the 1-direction during to loading in the 3-direction. The damaged modulus obtained from experiments is used to compute the damage parameter. For example

$$d_{11}^{11}=1-\frac{E_{11}^{d11}}{E_{11}} \tag{9}$$

The evolution of the damage parameters as a function of plastic strain is defined in a tabulated manner. The failure model is currently under development and is not discussed or utilized in this paper.

EXPERIMENTAL METHODS AND RESULTS

Table I shows how the experimental data for the deformation model can be obtained.

TABLE I. REQUIRED TESTS AND RESULTING INPUT FOR MAT213 [5]

Test	**ASTM Standard**	**Resulting Input for MAT213**
Tension 1-direction	D3039	Tension stress-strain curve σ_{11}^{T} vs ε_{11}^{T}
		Yield strain $\left(\varepsilon_{11}\right)_{y}^{T}$ and yield stress $\left(\sigma_{11}\right)_{y}^{T}$
		Elastic Poisson's ratio $\left(\nu_{12},\nu_{13}\right)$
		Plastic Poisson's ratio $\left(\nu_{12}^{p},\nu_{13}^{p}\right)$
Tension 2-direction	D3039	Tension stress-strain curve σ_{22}^{T} vs ε_{22}^{T}
		Yield strain $\left(\varepsilon_{22}\right)_{y}^{T}$ and yield stress $\left(\sigma_{22}\right)_{y}^{T}$
		Elastic Poisson's ratio $\left(\nu_{23}\right)$
		Plastic Poisson's ratio $\left(\nu_{21}^{p},\nu_{12}^{p}\right)$
Tension 3-direction	D7291	Tension stress-strain curve σ_{33}^{T} vs ε_{33}^{T}

		Yield strain $\left(\varepsilon_{33}\right)_y^T$ and yield stress $\left(\sigma_{33}\right)_y^T$
		Plastic Poisson's ratio $\left(\nu_{32}^p, \nu_{31}^p\right)$
Compression 1-direction	D3410	Compression stress-strain curve σ_{11}^C vs ε_{11}^C
		Yield strain $\left(\varepsilon_{11}\right)_y^C$ and yield stress $\left(\sigma_{11}\right)_y^C$
Compression 2-direction	D3410	Compression stress-strain curve σ_{22}^C vs ε_{22}^C
		Yield strain $\left(\varepsilon_{22}\right)_y^C$ and yield stress $\left(\sigma_{22}\right)_y^C$
Compression 3-direction	D7291	Compression stress-strain curve σ_{33}^C vs ε_{33}^C
		Yield strain $\left(\varepsilon_{33}\right)_y^C$ and yield stress $\left(\sigma_{33}\right)_y^C$
Shear 1-2 plane	D5379/M-12	Shear stress-strain curve σ_{12} vs ε_{12}
		Yield strain $\left(\varepsilon_{12}\right)_y$ and yield stress $\left(\sigma_{12}\right)_y$
Shear 2-3 plane	D5379/M-12	Shear stress-strain curve σ_{23} vs ε_{23}
		Yield strain $\left(\varepsilon_{23}\right)_y$ and yield stress $\left(\sigma_{23}\right)_y$
Shear 1-3 plane	D5379/M-12	Shear stress-strain curve σ_{31} vs ε_{31}
		Yield strain $\left(\varepsilon_{31}\right)_y$ and yield stress $\left(\sigma_{31}\right)_y$
Off-axis tension (45^0, 1-2 plane)	D3039	Off-axis tension stress-strain curve σ_{45}^{1-2} vs ε_{45}^{1-2}
		Yield strain $\left(\varepsilon_{45}^{1-2}\right)_y$ and yield stress $\left(\sigma_{45}^{1-2}\right)_y$
Off-axis tension (45^0, 2-3 plane)	D3039	Off-axis tension stress-strain curve σ_{45}^{2-3} vs ε_{45}^{2-3}
		Yield strain $\left(\varepsilon_{45}^{2-3}\right)_y$ and yield stress $\left(\sigma_{45}^{2-3}\right)_y$
Off-axis tension (45^0, 1-3 plane)	D3039	Off-axis tension stress-strain curve σ_{45}^{1-3} vs ε_{45}^{1-3}
		Yield strain $\left(\varepsilon_{45}^{1-3}\right)_y$ and yield stress $\left(\sigma_{45}^{1-3}\right)_y$

There are no ASTM standards for damage characterization tests and the tests were developed to obtain the damage parameter versus total strain data.

Experimental Equipment

Both force and strain data were gathered continuously throughout the duration of each test. Force data was gathered using the load cell built into an MTS 810 universal test frame. Full field strain data was gathered using digital image correlation (DIC). The test frame, load cell, and DIC camera equipment are shown in Figure 2.

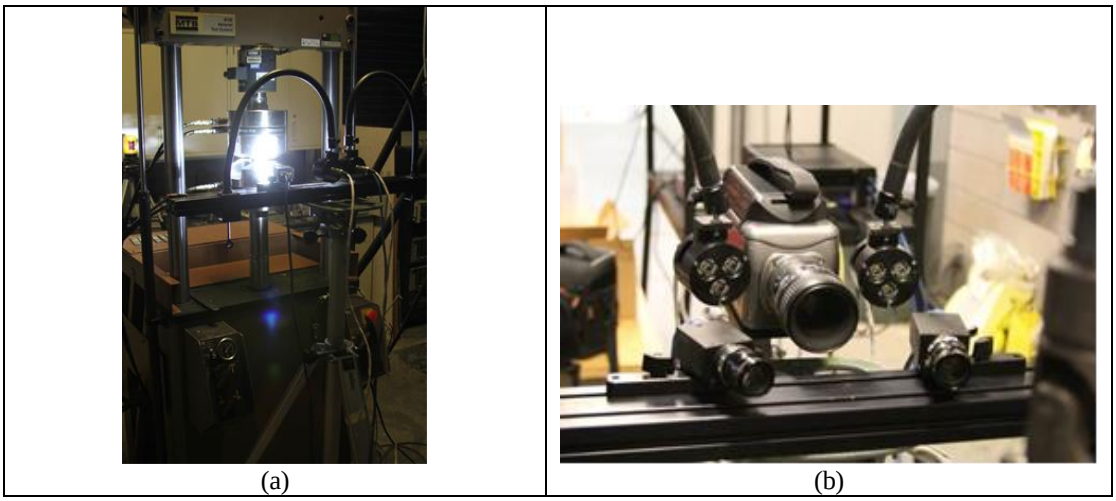

(a) (b)

Figure 2. (a) Load frame and (b) DIC cameras used in experiments

The experiments used to generate the required input can be placed into 4 categories: in-plane tension/compression tests, through thickness compression tests, through thickness tension tests, and shear tests. All tests in a given category use similar fixtures. In-plane tension and compression tests are performed using MTS 647.10A hydraulic wedge grips. The hydraulic grips were used because the in-plane tension and compression specimens require relatively high forces to induce failure in the specimen and the hydraulic system provides sufficient gripping pressure to allow the specimens to reach those forces without slipping. Both in-plane and through-thickness shear tests are performed using the Iosipescu shear fixture. Through-thickness compression tests were performed using specially machined A2 tool-steel platens with notches etched into the surface for alignment purposes. Finally, through thickness tension tests were performed using a custom designed fiberglass gripping system. The test fixtures are shown in Figure 3.

(a) (b)

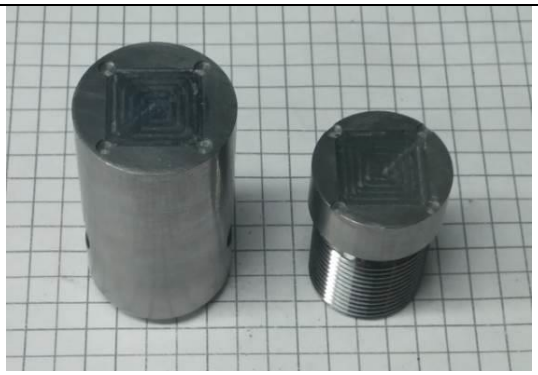

(c)

Figure 3. (a) Hydraulic grips, (b) Iosipescu shear fixture, and (c) compression tabs

Post-processing Experimental Data

After loading a specimen to failure, Vic-3D [6] was used to process images of the specimen using DIC at various stages of the test. A representative area, away from the specimen boundaries, was used to gather the strain data for the experiment. The force data is then used to compute the stress in the specimen using the average cross-sectional area of the gage section of the specimen and assuming a purely uniaxial state of stress. After performing multiple replicates of a test and generating the stress-strain curve, a single representative model curve, which is used as input to drive MAT 213, is generated by obtaining an unweighted average of the individual stress-strain curves.

Experimental Results

After performing multiple replicates of each test, a model curve was generated to be used as input for MAT 213. For the sake of brevity, only a few of the 12 QS-RT stress-strain curves are shown in Figure 4.

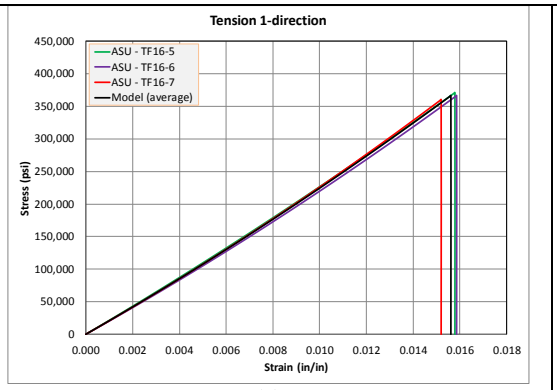

(a)

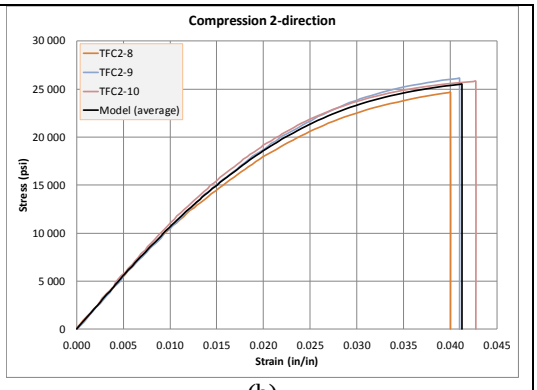

(b)

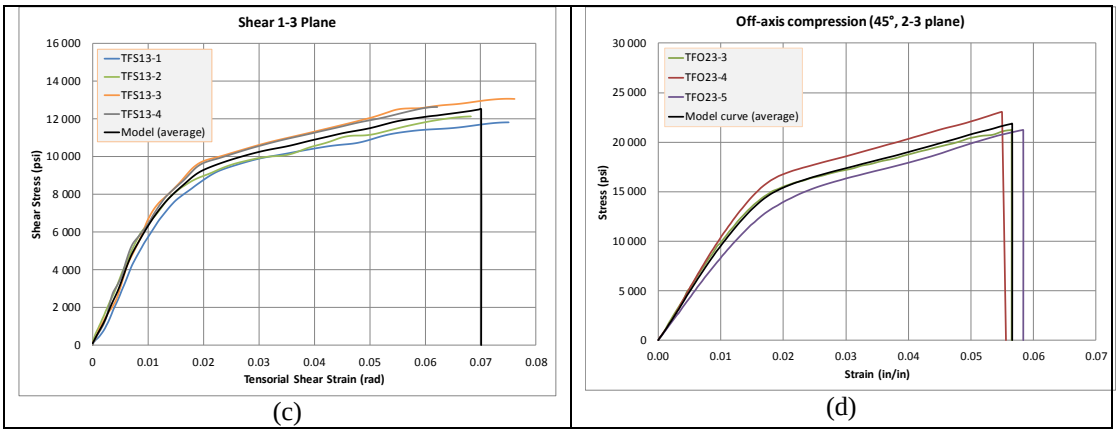

Figure 4. Complete stress-strain curves obtained from (a) 1-direction tension test, (b) 2-direction compression test, (c) 1-3 plane shear test, and (d) 2-3 plane 45^0 off-axis compression test

In addition to the stress-strain curves shown in Figure 4, other material parameters can be derived from the experimental data including the elastic moduli and the elastic and plastic Poisson's ratios (used for computing the coefficients in the flow law) as shown in Table II.

TABLE II. SUMMARY OF DERIVED MATERIAL PROPERTIES

Property	Value
E_{11} Tension	23 457 871 psi
E_{22} Tension	1 066 413 psi
E_{33} Tension	966 505 psi
E_{11} Compression	18 775 652 psi
E_{22} Compression	1 119 123 psi
E_{33} Compression	906 423 psi
G_{12}	579 489 psi
G_{23}	331 021 psi
G_{13}	347 738 psi

Property	Value
ν_{12} Tension	0.317
ν_{21} Tension	0.0168
ν_{32} Tension	0.439
ν_{31} Tension	0.027
ν_{12} Compression	0.342
ν_{21} Compression	0.0207
ν_{32} Compression	0.685
ν_{31} Compression	0.039
ν_{12}^{p} Tension	-
ν_{21}^{p} Compression	0.0141
ν_{32}^{p} Compression	0.776
ν_{31}^{p} Compression	0.025

Additional Input Parameters

The final parameters needed populate material model input, are the plastic potential function coefficients. The calculation of these coefficients for the T800/F3900 composite was performed in [3] with the summary of the coefficients determined with the experimental data shown in Table III. The values H_{11}, H_{12} and H_{13} are all equal to zero due to the elastic brittle behavior of the composite in the fiber or 1-direction, which is evident in Figure 4(a). The values H_{22} and H_{33} are equal to 1.0 as the master plastic cases, with H_{23} calculated from the 3-2 plastic Poisson's ratio in Table II. Finally, the values H_{44}, H_{55} and H_{66} were determined from the fitting procedure described in [3].

TABLE III. SUMMARY OF CALCULATED PLASTIC POTENTIAL COEFFICIENTS

Plastic Potential Coefficient	Value
H_{11}	0.0
H_{22}	1.0
H_{33}	1.0
H_{12}	0.0
H_{23}	0.776
H_{13}	0.0
H_{44}	4.239
H_{55}	15.31
H_{66}	5.372

Finally, results from one of the damage characterization tests (uncoupled shear 1-2 plane, where the damage in the 1-2 direction is tracked as a function of the strain in the 1-2 direction) is shown in Figure 5.

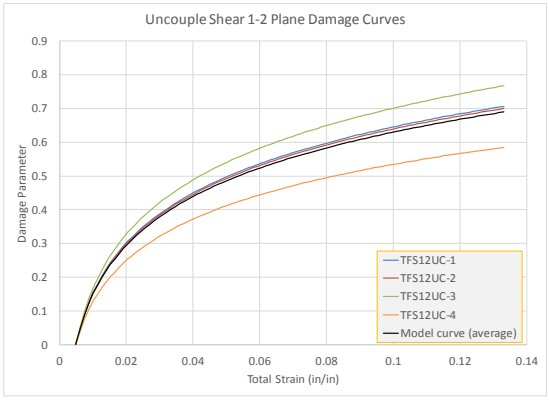

Figure 5. Uncoupled shear 1-2 plane damage parameter versus total strain curve

VERIFICATION TESTS

A series of one-element verification tests were conducted to ensure that the MAT213 implementation and characterization was correctly done. For the sake of brevity, the finite element model and results from two tests are shown in Figure 6.

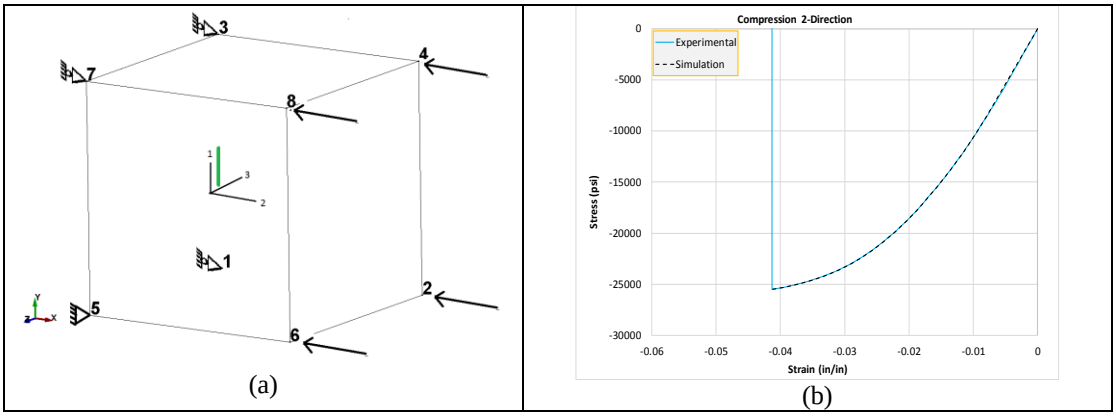

(a) (b)

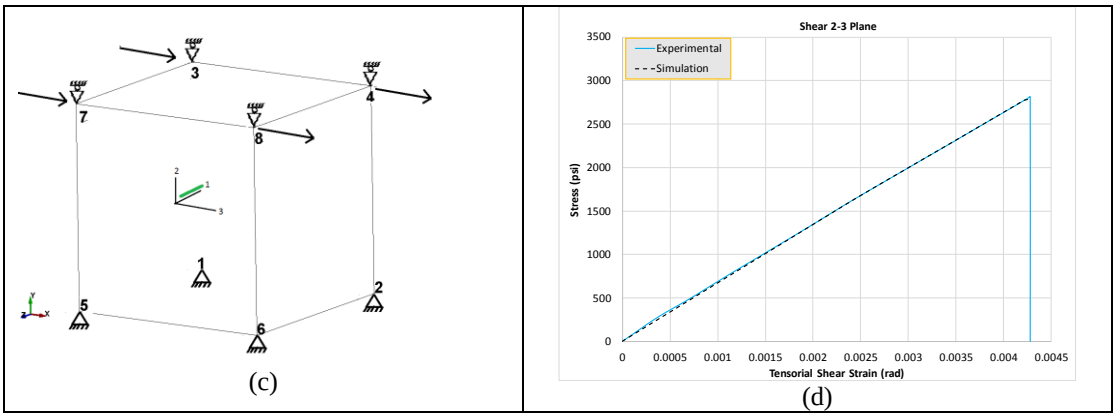

Figure 6. One-element verification tests (a) FE model for 2-direction compression test, (b) results from verification test, (c) FE model for 2-3 plane shear test, and (d) results from verification test

The verification test results show that the input and the generated curves match indicating that the implementation of the theory in the computer code and the characterized input parameters are correct.

VALIDATION TEST

An impact test was conducted at NASA Glenn Research Center. A 304.8 mm x 304.8 mm x 3.10 mm T800/F3900 composite flat panel fabricated with 16 plies, was subjected to a low velocity impact using an aluminum impactor. The unidirectional panel was such that the fibers in the panel were oriented vertically (see Figure 7 and [2]). Table IV shows the details of the impactor.

TABLE IV. IMPACTOR DETAILS

Impactor Properties	Value
Horizontal Velocity, ft/s	27.4
Pitch, deg.	4.33
Mass, gm	50.0

An LS-DYNA model was built with the details as close to the impact test as possible. The T800/F3900 properties obtained as explained earlier (stress-strain curves, other material properties and damage versus total strain curves) were used as MAT213 input. The FE model of the composite plate has 214,000 8-noded solid elements with three layers of elements through the thickness. The nodes on the surface of the bolt holes were completely restrained in the x-y-z directions. Figure 7 shows the details of the FE model.

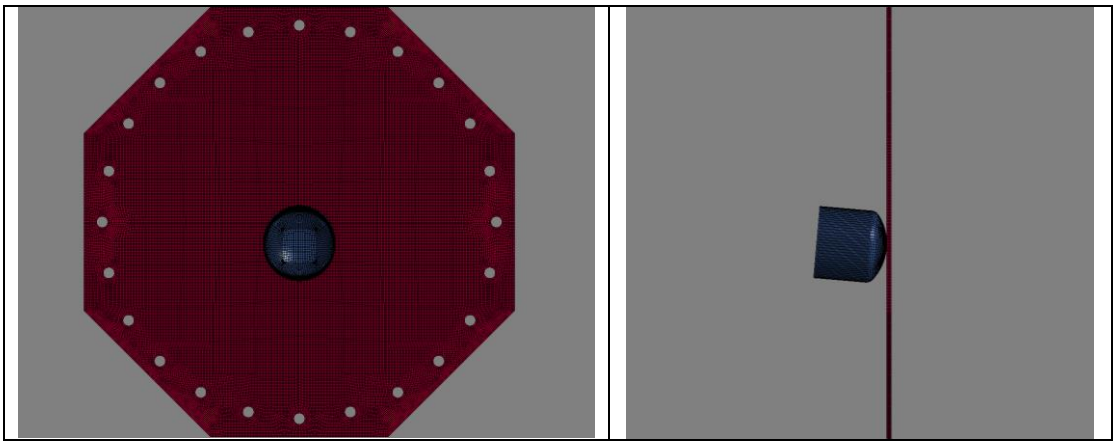

Figure 7. FE Model of the impact test

The out-of-plane displacements at the center as well as the maximum out-of-plane displacement of the plate for the FE simulation as well as those obtained from the test are compared with the physical test in Figure 8.

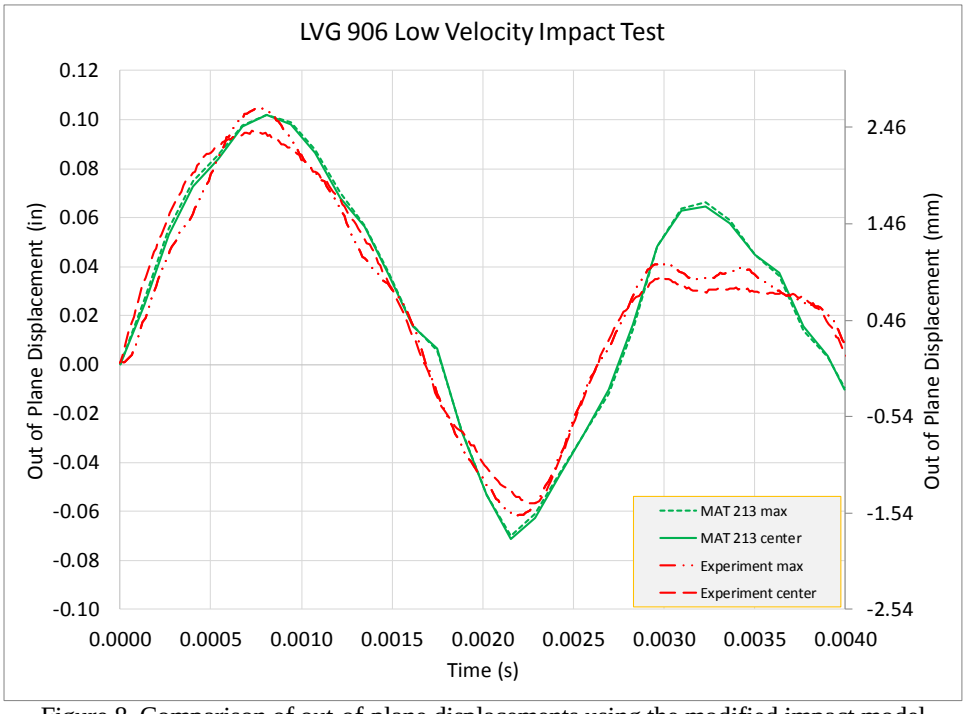

Figure 8. Comparison of out-of-plane displacements using the modified impact model

The comparison show that the FE predictions are reasonably close to the experiment for the first positive and negative peak values and times. It appears that the prediction of the second positive peak is not as good possibly due to approximations made in the FE model – some of the elements of the test fixture are excluded from the model, the estimated value of the coefficient friction between the impactor and the plate, the nonzero rotational velocities of the impactor, etc.

CONCLUSIONS

In this paper a newly developed orthotropic material model for use in modeling impact tests is discussed. Details of the three steps in using the material model with some confidence are presented. The experimental plan is used to generate the data for the deformation and damage parts of the model. The verification tests are used to ascertain if the code implementation is code. And finally, the validation test is used to gain confidence in the predictive capabilities of the developed constitutive model.

Results from the implementation into a special version of LS-DYNA show that the developed and implemented model can be used as a predictive tool.

ACKNOWLEDGEMENTS

Authors Hoffarth, Khaled, Shyamsunder and Rajan gratefully acknowledge the support of (a) the Federal Aviation Administration through Grant #12-G-001 titled "Composite Material Model for Impact Analysis", William Emmerling, Technical Monitor, and (b) NASA through Contract Number: NN15CA32C titled "Development and Implementation of an Orthotropic Plasticity Progressive Damage Model for Transient Dynamic/Impact Finite Element Analysis of Composite Structures", Robert Goldberg, Contracting Officer Representative.

REFERENCES

1. Goldberg, R., Carney, K., DuBois, P., Hoffarth, C., Harrington, J., Rajan, S., & Blankenhorn, G. (2016). Development of an Orthotropic Elasto-Plastic Generalized Composite Material Model Suitable for Impact Problems. *ASCE J of Aerospace Engineering*, *29*(4).

2. Hoffarth, C., Rajan, S. D., Goldberg, R. K., Revilock, D., Carney, K. S., DuBois, P., & Blankenhorn, G. (2016). Implementation and validation of a three-dimensional plasticity-based deformation model for orthotropic composites. *Composites Part A: Applied Science and Manufacturing*, *91*(1), 336-350.

3. Hoffarth, C., Khaled, B., Shyamsunder, L., Rajan, S. D., Goldberg, R. K., Carney, K. S., DuBois, P., & Blankenhorn, G. (2017). Verification and Validation of a Three-Dimensional Orthotropic Plasticity Constitutive Model Using a Unidirectional Composite. *Fibers*, *5*(1), 1-13.

4. LSTC (2017). LS-DYNA R8, http://lstc.com/products/ls-dyna (accessed 10 June 2017).

5. Harrington, J., Hoffarth, C., Rajan, S.D., Goldberg, R., Carney, K., DuBois, P. and Blankenhorn, G. (2017). Using Virtual Tests to Complete the Description of a Three-Dimensional Orthotropic Material, *ASCE J of Aerospace Engineering*, DOI: 10.1061/(ASCE)AS.1943-5525.0000737.

6. Correlated Solutions Inc. (2017). http://correlatedsolutions.com/vic-3d/